DOI https://doi.org/10.15589/znp2021.1(484).18
UDC 502:51:504.5

NUMERICAL ANALYSIS OF KEROSENE SPRAY COMBUSTION IN VARIOUS INJECTION PREPARATIONS AND EMISSION BEHAVIOUR ASSESSMENT

ЧИСЕЛЬНИЙ АНАЛІЗ ВПЛИВУ РІЗНИХ УМОВ ВПОРСКУВАННЯ ГАСУ НА ПРОЦЕС ЙОГО ЗГОРЯННЯ І УТВОРЕННЯ ВИКИДІВ В КАМЕРІ ЗГОРЯННЯ

Masoud Hajivand
m.hajivand82@gmail.com
ORCID: 0000-0002-9990-9761
Dmytro A. Dolmatov
d.dolmatov@khai.edu
ORCID: 0000-0002-7268-1509

М. Хаджіванд,
аспірант
Д. А. Долматов,
докт. техн. наук, доцент

National Aerospace University "Kharkiv Aviation Institute", Kharkiv
Національний аерокосмічний університет імені М. Є. Жуковського «Харківський авіаційний інститут», м. Харків

Abstract. This paper presents a numerical analysis of liquid kerosene combustion, by means of variation of liquid kerosene droplets sizes and injection angles, through an atomizer, into a real combustor. The droplets are considered, through the Rosin Rammler droplet particles size distribution.
The main purpose of this investigation is to evaluate the combustor outlet temperature and NO concentration, with regard to droplet evaporation time and distance, during the combustion process, and to predict CO and NO concentration and temperature behaviour, in the primary zone of combustion. Due to the complexity of the numerical simulation of two-phase flows, such as combustion of liquid fuels, grid independence is considered, using structured and unstructured grids, including, with and without the radiation effect modelling. For the simulation of evaporated kerosene combustion, the flamelet model was performed for the detailed kinetic scheme of chemical reactions between kerosene and air, which is integrated in ANSYS CFX, including the thermal and prompt prediction of NO.
The standard k-ϵ turbulence model was used with enhanced wall treatment.
In this study, the Eulerian-Lagrangian Spray Atomization model is implemented as a Computational Fluid Dynamics (CFD) tool for the prediction of spray behaviour.
Verification and validation of analysis results, were considered in this study where the results, such as outlet and wall temperature of the combustor, were compared with the real experimental results.
The results of this investigation show that, by increasing the liquid kerosene droplet sizes, temperature, NO formation levels and CO concentration rise, in combustion primary zone and at the exit section of combustor, and increasing the fuel spray cone angle causes to increase the temperature and NO concentration in combustor outlet. In the combustion primary zone, by increasing the spray cone angle the CO formation gives the lower value, except in the primary zone of droplet evaporation, due to the not fully vaporized droplets. So, by increasing the spray cone angle the NO concentration and temperature value rise in the distances (15 mm to 55 mm), while these values are lower in the distances (75 mm to 120 mm), due to the mixing quality and not fully droplet vaporization.
Key words: combustor; emission; kerosene droplets; numerical analysis; evaporation; radiation; Rosin Rammler.

Анотація. У цій статті представлений чисельний аналіз впливу розмірів крапель рідкого гасу та кутів впорскування через розпилювач на процес горіння рідкого гасу в реальній камері згоряння.
Краплі розглядаються за допомогою розподілу часток за розмірами Розіна Раммлера. Основна мета цього дослідження – оцінити температуру на виході з камери згоряння і концентрацію NO з урахуванням часу і відстані випаровування крапель під час процесу згоряння, а також спрогнозувати концентрацію CO і NO і температуру в першій зоні згоряння. Через складність чисельного моделювання двофазних потоків, таких як горіння рідкого палива, в розрахунковому дослідженні використовуються структуровані і неструктуровані сітки, з урахуванням і без урахування моделювання випромінювання. Для моделювання горіння випаруваного гасу була виконана модель flamelet для детальної кінетичної схеми хімічних реакцій між гасом і повітрям, яка

інтегрована в ANSYS CFX, включаючи термічний і швидкий механізм утворення NO. Використана стандартна модель k-є турбулентності з поліпшеною обробкою стінок.
У цьому дослідженні як інструмент обчислювальної динаміки рідини (CFD) для прогнозування поведінки розпилення реалізована модель розпилення Ейлера-Лагранжа.
Верифікація отриманих результатів виконана шляхом порівняння температури на виході і температури стінок камери згоряння з реальними експериментальними даними.
Результати дослідження показують, що збільшення розміру крапель рідкого гасу призводить до підвищення температури та рівня утворення NO та CO в первинній зоні згоряння та на виході із зони згоряння, а також збільшення кута розпилення палива спричиняє підвищення температури і концентрації NO на виході з камери згоряння. У первинній зоні горіння збільшення кута конуса розпилення призводить до зниження CO, за винятком первинної зони випаровування крапель, через неповне випаровування крапель. Таким чином, у разі збільшення кута розпилювального конуса концентрація NO та значення температури зростають на відстані від 15 мм до 55 мм, тоді як ці значення нижчі на відстанях від 75 мм до 120 мм, завдяки якості змішування та неповного випаровування крапель.
Ключові слова: камера згоряння; емісія; крапельки гасу; чисельний аналіз; випаровування; радіація; Розін Раммлер.

FORMULATION OF THE PROBLEM

In the complete combustion of hydrocarbon fuels, the exhaust gas from the gas turbine combustors, contains the components, such as. oxygen (O2), nitrogen (N2), carbon dioxide (CO2), and water steam (H2O), which in real combustion, however carbon monoxide (CO), unburned hydrocarbons (HC), hydrogen (H2), nitrogen oxide (NOx), and particulates also appear in addition to the above components in the combustion products [1].

Pollutant emissions from combustion processes of hydrocarbon fuels have become of great public concern due to their impact on human health and the environment. The past decade has witnessed rapid changes both in the regulations for controlling gas turbine emissions and in the technologies used to meet these regulations [2].

For high efficiencies of combustion, high temperatures are necessary, but NOx emissions increase exponentially with temperature and linearly with residence time. Concerning carbon monoxide emissions, increasing the residence time is favourable for CO oxidation to CO2, and reducing the combustion temperature can increase CO, due to local extinction [3].

Since gas turbine combustors operate in the non-premixed mode for safety and stability [4; 5], unfortunately, this mode leads to unacceptably high levels of thermal NOx, which is produced in the high-temperature, near-stoichiometric regions that occur in the combustor during the mixing of fuel and air [6].

Traditional methods that have been used to moderate the temperature and control thermal NOx formation include steam or water injection and Rich/Quench/Lean (RQL) combustion [4; 5].

However, injection of steam or water lowers the process efficiency and increases emissions of CO and unburned hydrocarbons (UHC), and the effectiveness of RQL combustion is limited by the rate at which air can be mixed with hot gases in the lean zone. Although regulations limiting NOx emission are site-specific [7], the general objective of the gas turbine industry is to achieve levels of less than 10 ppm (at 15% O2) [8; 9]. Achieving this “ultra-low” level of NOx is not feasible by traditional methods.

Beside the methods described above, combustion engineers regard the fuel preparation process and fuel spray modification as one that must necessarily play a key role in achieving the reduction of harmful substances and emissions [10]. The liquid fuels employed in liquid fuel combustors must first be atomized before being injected into the combustion zone. The spray properties of most relevance to the formation of pollutant emissions are mean drop size, drop size distribution, cone angle, and other properties of special importance for the successful modelling of spray characteristics include droplet and gas velocities, droplet trajectories, and mass flux distributions [10].

As an example, for the ignition of a fuel spray it is the initial rate of evaporation that is important, whereas for high combustion efficiency the time required for complete evaporation of the fuel spray is the dominant factor. Another example is provided by the lean premix-prevaporize combustor. A key feature of this concept is the attainment of complete evaporation of the fuel and complete mixing of the fuel vapor with air prior to combustion, thus failure to fully vaporize the fuel results in higher NO, emissions. It is important, therefore, to know how the fraction or percentage of fuel evaporated varies with time, so that the best compromise can be made between the conflicting requirements of minimum NOx emissions and minimum length of premixing chamber [11].

Atomization characteristics affects emission levels, such as formation of NO, through the evaporation and mixing quality of injector. Commonly, the influence of atomization quality is most obvious at slightly fuel-lean conditions, with reduced drop sizes, in spite of cone angle and velocity of droplets injection, leading to reduce emissions [12].

This emission reduction is attributed to the more uniform fuel dispersion and higher evaporation rates

that are characteristic of small drops, and which cause a larger proportion of the total burning process to occur in a premixed, rather than a diffusion, mode [12].

ANALYSIS OF RECENT RESEARCH AND PUBLICATIONS

Fluid flow within the combustor includes the complexities of combustion processes, turbulence, heat transfer, phase change, and mass transfer. For this reason, accurate knowledge of the flow field requires, accurate modelling of the flow inside the combustor. Due to the complexity of the flow, recognizing the flow fields is possible, only with advanced three-dimensional numerical methods.

Although, research on liquid fuel combustors, has provided researchers, with a wealth of information in this area, but how-to distribution fuel injection output from fuel injection systems and the process of mixing which has a significant effect on the quality of combustion and the amount of pollutant emissions, should be further investigated.

Therefore, the present work is defined to investigate the effect of fuel injection indices on the process of fuel-air mixture formation, with respect to the details of fuel injection, and combustion and pollution process, using different rates of fuel injection, different timing, during liquid fuel spraying.

In 1979 and 1982, Nizami et al. [13; 14] discuss experimental results of NO and NOx emissions from the atmospheric, monodisperse fuel spray combustion of different hydrocarbon fuels. The authors observed a significant effect of droplet size, with NO and NOx reaching minima around a droplet size of 48 to 55μm. These minima shift towards a smaller droplet size for single component fuels of lower vapor pressure. Prevaporization in the spray and the transition from diffusive to pre-vaporized, premixed combustion are considered important factors in determining the minimum NOx point [15].

K.K. Rink and A.H. Lefebvre in 1989 [12] in their investigation reported that atomization quality affects NO emission levels through the evaporation and mixing characteristics of the spray. Generally, the influence of atomization quality is most apparent at slightly fuel-lean conditions, with reduced drop sizes leading to diminished NO, CO and UHC emissions.

This reduction in NO is attributed to the more uniform fuel dispersion and higher evaporation rates that are characteristic of small drops, and which cause a larger proportion of the total burning process to occur in a premixed, rather than a diffusion, mode. The reason behind this observation is that small droplets have short evaporation times, and consequently, they have enough time to mix with air before igniting, leading to partial premixing which is known to burn more efficiently compared to mixtures found in pure non-premixed configurations [16].

The fuels employed in their study included diesel oil (DF 2), a low aromatics kerosine (JP 7), a shale-derived JP 4, a fuel containing 28 percent of monocyclic aromatics (FL-0654), and a fuel containing 27 percent of dicyclic aromatics (FL-0653).

Abrishamchi et al. [17] used liquid fuel to study the emission of NOX and CO produced from a cylindrical furnace with various angles and patterns of fuel spray were studied through the experimental method. Pollutant's measurement has been done for fuel spray angles of 45°, 60°, and 80° for spray pattern of a hollow and solid cone. They found that increasing the spray angle caused a decrease in CO emission and an increase in NOx.

When the spray angle increases, the diameter of the fuel particles exhausted from the nozzle decrease, which results in increasing the contact between fuel droplets and the air molecules, and as a result, the air-fuel mixing will also increase. Better air-fuel mixing will create a homogenous mixture that increases combustion efficiency and hence, increasing combustion temperature and NOx.

Khazraii et al. [18] simulated NOx emissions numerically in a turbulent liquid fuel spray flames using thermal and fuel models. The study investigated the influence of fuel spray angle (45°, 60°, and 80°) and the inlet air temperature on the emitted nitric oxides. They found that with increasing in spray angle, NOx emission increased.

Effect of fuel spray cone angle in an aero-gas turbine combustor has been studied by R.K. Mishra et al. [19], using computational fluid dynamics (CFD), for a 22.5° sector of an annular combustor, for the various injection angles, 60° to 140°, using the eddy dissipation combustion model in ANSYS CFX computational package.

The results of investigation proved that at higher spray cone angle, the flame and high-temperature zone moves upstream close to atomizer face and a uniform flame is sustained over a wide region causing better flame stability.

THE AIM OF THE STUDY

The ***purpose of this investigation*** is to define the emission characteristics of liquid kerosene combustion at the outlet, including in the primary zone of combustion, in a real combustor, through the various injection conditions, with the help of Computational fluid dynamics (CFD) numerical analysis, including the droplet vaporization behaviour, and their trajectories, during the combustion process, such as droplet evaporation time and distance.

THE MAIN MATERIAL

Refer to the previous study [20], the fuel injection parameters, in this study, were implemented without the primary and secondary breakup model, by the initial size distribution of the droplets in the spray following atomization is considered using the Rosin Rammler distribution function.

Due to the real experiment data [21; 22; 23], in a real combustor, the verification and validation results of this study is presented.

P. Ghose et al. [21; 22; 23] presented a 3-D model of the real combustor which is illustrated in Fig. 1. The combustion chamber is 100 mm in diameter and 500 mm in length from the plane of the swirler.

The inlet plane to the computation domain is considered at 40 mm upstream to the swirler plane, both in the primary and secondary air streams.

The boundary conditions of the experiment are: total mass flow rate of air is set to 0.04 kg/s at 300 K, resulting in an overall air-fuel ratio of 110 by mass. The air has been split to 50% for each air inlet primary and secondary. However, the inlet boundaries for air are specified 40 mm before the actual entry to the combustor zone. The swirl number for the primary air is set to 2.142 and for secondary air is 0.

The kerosene droplets have been considered with the dispersion angle of 6° over a half cone angle of 18° and the injection pressure differential is taken as 6 bars. Fuel flow rate from the injector having orifice diameter of 0.25 mm has been taken as 0.00036 kg/s with the inlet fuel temperature of 300 K.

All simulation results presented in this work were obtained using the commercial computational fluid dynamics (CFD) code ANSYS CFX [24; 25].

This report presents a numerical investigation of kerosene fuel spray combustion of a real combustor.

Jet-A aviation fuel (kerosene), modelled as a two-component surrogate fuel (by mass 60% C10H22 and 40% C9H12). The standard k–ε model with the enhanced wall treatment and the Euler-Lagrange method were employed for the simulation of the turbulence and spray. k–ε model is most popular two-equation model, which is still commonly used, introduced by Jones and Launder [26; 27].

Set of differential equations which describes fluid motion are Navier-Stokes equations and conservation of mass. Energy and mass transfer equation can be added to these equations depend on the nature of problem. CFD methods tries to solve these equations over the calculation domain by considering specific boundary and initial conditions with numerical methods [28; 29; 30; 31; 32].

The most famous methods to calculate turbulence characteristics are Reynolds Average Navier-Stokes (RANS) models. In this model, attention is on the mean flow and the effects of turbulence on mean flow properties. This is done by introducing extra variables to the Navier Stokes equations which are related to interaction between various turbulent fluctuations.

According to the calculation of these extra variables, several RANS models have been obtained e.g., k–ε model and shear stress models (SST). The computational cost of these models is moderate and therefore they are widely used in the industries and academia [32].

In the laminar flamelet model available in ANSYS CFX, the species mean mass fractions are stored in the flamelet library as a function of the mean mixture fractions $\widetilde{Z}$, its variance $\widetilde{Z''^2}$ [25; 33]. The Favre mean species mass fraction can then be calculated with a probability density function $\widetilde{P}$ [25; 27].

$$\widetilde{Y}_i = \int_0^1 Y_i(Z, \tilde{\chi}_{st})\, \widetilde{P}(Z)\, dZ \qquad (1)$$

As shown here, typically, a β-function is used as the pdf of the mixture fraction is used, which in other words, it can be written like $\tilde{P}(Z, x, t)$. The pre-integration of flamelet tables is done with CFX-RIF [25] automatically.

Within the framework of the flamelet model, instead of solving the transport equation for each species, only the transport equations for the Favre mean mixture fraction and its variance are solved. Assuming that all species have equal diffusivities, the transport equation for the Favre mean mixture fraction can be written as [25; 27].

$$\frac{\partial\left(\bar{\rho}\tilde{Z}\right)}{\partial t} + \frac{\partial\left(\bar{\rho}\tilde{u}_j\,\tilde{Z}\right)}{\partial x_j} = \frac{\partial}{\partial x_j}\left[\left(\bar{\mu} + \frac{\mu_t}{\sigma_Z}\right)\frac{\partial\tilde{Z}}{\partial x_j}\right] \qquad (2)$$

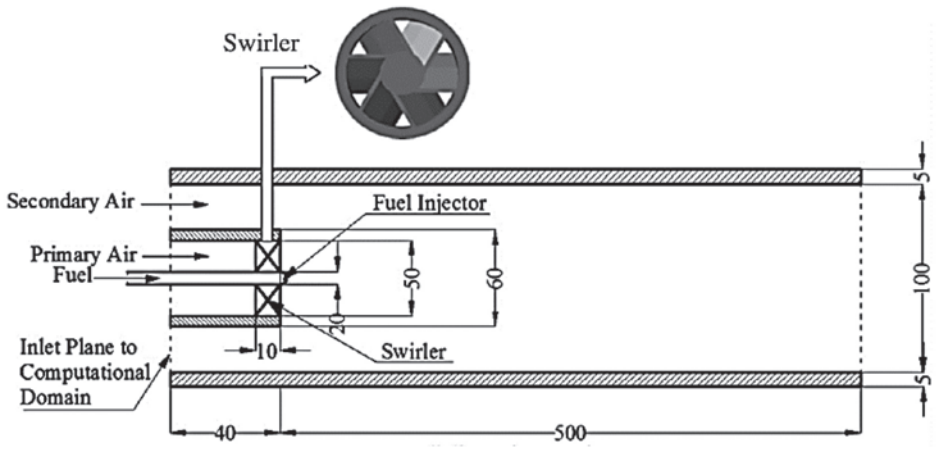

Fig. 1. Physical geometry of the real combustor under study (P. Ghose et al.)

Where μ is the molecular dynamic viscosity, μ_t – the turbulent viscosity and σ_Z is a model coefficient. As the mixture fraction is a conserved scalar, its transport equation contains no source term. The transport equation for the mixture fraction variance $\widetilde{Z''^2}$ can be modelled as follows [25; 27].

$$\frac{\partial\left(\bar{\rho}\widetilde{Z''^2}\right)}{\partial t}+\frac{\partial\left(\bar{\rho}\tilde{u}_j\,\widetilde{Z''^2}\right)}{\partial x_j}= =\frac{\partial}{\partial x_j}\left[\left(\bar{\mu}+\frac{\mu_t}{\sigma_{\widetilde{Z''^2}}}\right)\frac{\partial\widetilde{Z''^2}}{\partial x_j}\right]+2\,\frac{\mu_t}{\partial_Z}\left(\frac{\partial\tilde{Z}}{\partial x_j}\right)^2-\bar{\rho}\tilde{\chi} \tag{3}$$

where $\sigma_{\widetilde{Z''^2}}$ and $C\chi$ in formula (4) are model coefficients. The first term on the right-hand side represents the production of variance, whereas the last term models its dissipation. The instantaneous scalar dissipation rate $\tilde{\chi}$ is modelled as [27].

$$\tilde{\chi}=C_{\chi}\frac{\tilde{\varepsilon}}{\tilde{k}}\widetilde{Z''^2} \tag{4}$$

With $\tilde{\varepsilon}$ and $\tilde{k}$ being the dissipation rate and the turbulent kinetic energy, respectively. As the species mass fractions $\widetilde{Y_i}$ are previously stored in a flamelet table, they can be obtained within the CFD simulation by coupling the CFD code with the flamelet libraries as shown in Fig. 2 [34].

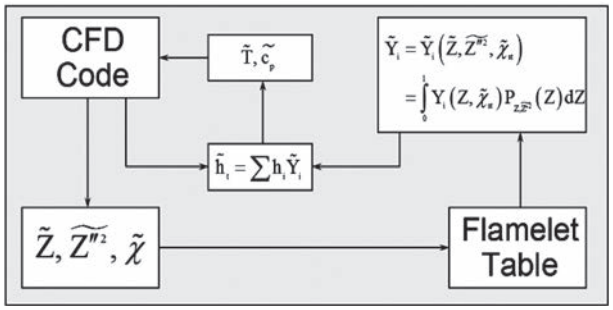

Fig. 2. Code structure of the flamelet model [34]

The properties Favre mean mixture fraction, mixture fraction variance and scalar dissipation rate are calculated from the CFD code. From these values, the pre-integrated mean values for the species mass fractions are then obtained by look-up in the flamelet library [27].

Heat transfer interacts with other physics when optimizing and verifying system and product designs. Radiation is one of them. Conduction, radiation, inter diffusion heat transfer occurs in the combustion system [35].

Since combustion is speedy oxidation generation of heat and radiation, is so important because of the intrinsic importance of chemical reaction. Thermal radiation is an important energy transport process at high temperature that needs to be considered for implementation of practical combustion system [35].

Radiation does not directly affect the reaction processes, but the transfer of radiation indirectly affects the flame temperature distribution and chemical reactions [35].

Chan and Viskanta in 2005 showed that Radiation can significantly affect the flame temperature, minor species, the NOx emissions, soot formation, flame extinction, and other phenomena.

The Differential Approximation or P1 model of radiation is also a simplification of the radiation transport Equation, which assumes that the radiation intensity is isotropic or direction independent at a given location in space. The full form of the radiant energy equation and the derivation of the P1 model for radiation are given in Modest [25; 36].

A brief summary is given in ANSYS CFX-Solver Theory Guide [25].

For the Discrete particles numerical modelling i.e., simulation of the fluid motion using the Euler-Lagrangian approach suggests a description of the multiphase interaction with special physical models [37].

Mass transfer between the phases is simulated through the liquid evaporation model implemented in CFX through the Antoine equation (Eq. (5)) is used to determine the boiling point of kerosene [38], which defines the mass transfer source term.

$$p_{\text{var}}=p_{scale}\cdot\exp\left(A-\frac{B}{T_p+C}\right) \tag{5}$$

Where, T_p stands for droplet temperature, p_{scale} is a scaling coefficient and A, B, C – empirical coefficients.

These coefficients are found in literature, and here, as kerosene (C10H22) is considered as the evaporating species, the values corresponding to kerosene are used [39].

Additional studies showed that variation of coefficients A, B, and C in the range of hydrocarbons close to kerosene does not influence the combustion efficiency significantly (less than 1.5% error) [37].

Using a Rosin-Rammler distribution for droplet sizes of the liquid coolant instead of uniform size distribution allows for convergence improvement without any impact on the integral parameters [37].

The Rosin-Rammler in Equation (6) initial size distribution, which is the most common nowadays for spray combustion cases and one of the cheapest, is used for both core-flow injections and coolant injections [37]:

$$f(d)=\frac{q}{D}\left(\frac{d}{D}\right)^{q-1}\cdot\exp\left[-\left(\frac{d}{D}\right)^{q}\right] \tag{6}$$

where D is the size parameter, q for spread parameter and d stand for droplet diameter [25].

The computations in the dispersed phase have been done to evaluate the interphase source terms for the gas phase conservation equations. In the dispersed phase, the spray is considered to comprise a finite number of droplet classes distributed over an initial dispersion angle.

The velocity, position, mass, and temperature histories of each of the droplet classes are traced along their trajectories using the respective conservation equations in a Lagrangian frame [40].

The trajectory of a droplet of the *k*th class is computed by evaluating the velocity and position of a representative droplet of the class along its motion. The velocity of the droplet is found out from the conservation of momentum equation considering only inertia and drag forces to be significant. The equation can then be written as:

$$m_d(k)\frac{d\,u_{d_i}(k)}{dt} = \\ = \frac{\pi}{8}\tilde{\rho}\left[d(k)\right]^2\left|u_i - u_{d_i}(k)\right|\left[u_i - u_{d_i}(k)\right]C_{drag} \quad (7)$$

The drag coefficient, C_{drag} ,is evaluated following the spherical drag low [40; 41].

Evaporation of the liquid from the surface of the droplets takes place considering the vapor pressure on the droplet surface to be equal to the saturation pressure at the droplet temperature [40].

A piecewise linear variation of the saturation pressure for the liquid fuel with temperature is considered for the evaluation. The mass transfer coefficient h_D is calculated from the Sherwood number correlation of Ranz and Marshall [42]. The change in droplet mass can therefore be accounted as:

$$\frac{dm_p}{dt} = \pi d_p^2 h_D\left(C_{f_s} - C_f\right) \quad (8)$$

where C_{f_s} and C_f are the mass fractions of the fuel vapor on the droplet surface and in the surrounding gas.

In order to find out the variation in temperature of the droplet along its trajectory, an energy balance across the droplet surface is considered as:

$$m_P\, c_{p_p}\frac{d\,T_P}{dt} = hA_P\left(T - T_P\right) - \frac{dm_P}{dt}\Delta H_V \quad (9)$$

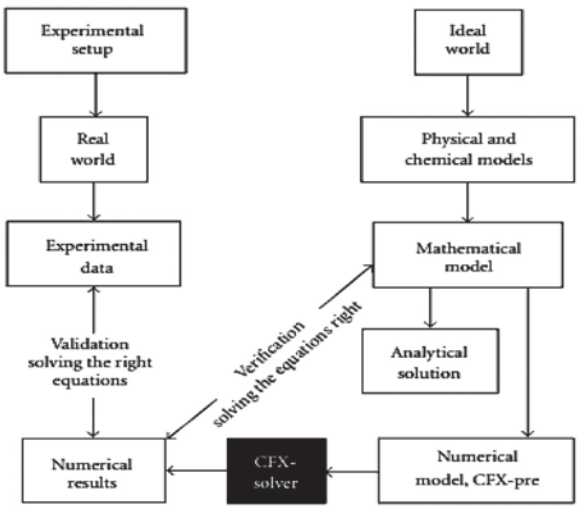

Fig. 3. Logic scheme of validation and verification [43]

The heat transfer coefficient (h) is found out from the Nusselt number correlation of Ranz and Marshall [42] and the radiation exchange with the gas phase is neglected.

Verification and validation are ground steps in obtaining a numerical solution (Fig. 2) [43]. The validation should be completed before obtaining the desired numerical results while the verification should be completed before the validation.

Normally, the whole numerical model, which includes equations of fluid dynamics, equation of state, and the model of turbulence and combustion, is already verified by the developer of the CFD code and the user should verify only its own user defined models [43].

Our ultimate aim is the modelling of the kerosene spray combustion, modelling the behaviour of droplets and the emission formations. For this purpose, we cannot rely on the predefined numerical model, but should use the models, which take into account the specifics of this complicated problem [43]. Thermal NO or Zeldovich NO (After Y.B. Zeldovich, 1946, who postulated the mechanism) is formed by the elementary reactions (Baulch et al. 1994) [44].

The thermal NO mechanism is a predominant source of NOx in gas flames at temperatures above 1800 K. The NO is formed from the combination of free radical O and N species, which are in abundance at high temperatures. The two-step mechanism, referred to as the Zeldovich mechanism, is thought to dominate the process, in (R1) and (R2) reactions [25]. In sub or near stoichiometric conditions, a third reaction may be important which is shown in reaction (R3).

When reaction (R3) is included with the first two, it is referred to as the extended Zeldovich mechanism. The name of thermal is used because the reaction rate of the first reaction has a very high activation energy due to the strong triple bond in the N2 molecules, and thus sufficiently fast only at high temperature [44].

The first reaction is the rate limiting step of the thermal NO formation. The rates of reactions (R1, R2, R3) are expressed below each of them.

$$O + N_2 \xrightarrow{k_1} NO + N \\ k_1 = \left(1.8\cdot 10^{11}\right)\exp\left(-\frac{38370}{T}\right) \quad (R1)$$

$$N + O_2 \xrightarrow{k_2} NO + O \\ k_2 = \left(6.4\cdot 10^{9}\right)\exp\left(-\frac{3162}{T}\right) \quad (R2)$$

$$N + O_2 \xrightarrow{k_3} NO + O \\ k_3 = 3.0\cdot 10^{3} \quad (R3)$$

When multiplied by the concentrations of the reactants, they yield rates in terms of $\left[kmol\ /\ m^3\ /\ s\right]$, which can be converted to a volumetric mass source term [25].

For the rate of formation of NO one obtains according to the reactions (R1, R2, R3):

$$\frac{d[NO]}{dt} = k_1[O][N_2] + k_2[N][O_2] + k_3[N][OH] \quad (13)$$

Because

$$\frac{d[NO]}{dt} = k_1[O][N_2] - k_2[N][O_2] - k_3[N][OH] \quad (14)$$

As described in [25], the thermal formation in $kg / m^3 / s$, $S_{NO,thermal}$, is therefore related to the rate of Reaction (R1):

$$S_{NO,thermal} = 2W_{NO}k_{thermal}[O][N_2]$$
$$k_{thermal} = k_1 \quad (15)$$

Here, denotes the molecular mass of NO. Thus, if the molar concentrations [O] and [N2] of O radicals and N2 are known, the thermal NO mechanism can be calculated [25].

When using the Laminar Flamelet model, almost always the O radical concentration can be taken without further assumptions from the solution because the model predicts it directly [25].

Prompt formation of NO occurs when temperatures lower than 1800 K.

Hydrocarbon flames tend to have an NO concentration that is too high to be explained with the Zeldovich mechanisms.

Hydrocarbon radicals can react with molecular nitrogen to form HCN, which may be oxidized to NO under lean flame conditions [25].

$$CH + N_2 \rightarrow HCN + N \quad (R4)$$

$$HCH + O_2 \rightarrow NO + ... \quad (R5)$$

The complete mechanism is very complicated. However, De Soete (see also Peters and Weber, 1991) proposed a single reaction rate to describe the NO source by the Fenimore mechanism, $S_{NO,prompt}$

$$S_{NO,prompt} = W_{NO}k_{prompt}[O_2]^{1/2}[N_2][Fuel]\left(\frac{w}{\rho}\right)^{3/2} \quad (18)$$

$$k_{prompt} = A_{prompt}\exp\left(-T_{A,prompt} / T\right) \quad (19)$$

W_{NO} and w denote molar mass of NO and the mean molar mass of the mixture, respectively. The Arrhenius coefficients depend on the fuel [25].

The formation of NO is a slow press which kinetically rate limited. Unlike other spices the mean value of NO cannot be obtain from flamelet library using equation (1) [45].

When modelling NO*x* formation in kerosene/air combustion, the thermal NO and prompt NO are taken into account.

In the simulation process, we solve the mass transport equation for the NO species, taking into account convection, diffusion, production and consumption of NO and related species. This approach is completely general, being derived from the fundamental principle of mass conservation. For thermal and prompt NO*x* mechanisms, only the following NO species transport equation is needed [46]:

$$\rho\frac{\partial Y_{NO}}{\partial t} + \rho u_i\frac{\partial Y_{NO}}{\partial x_i} = \frac{\partial}{\partial x_i}\left(\rho D\frac{\partial Y_{NO}}{\partial x_i}\right) + S_{NO} \quad (20)$$

The source term S_{NO} is to be determined for different NOx mechanism.

Grid generation or meshing is a very critical part within the CFD simulation process as it not only dictates the simulation time but also the accuracy of results of the study.

Generating a very coarse and poor-quality mesh or grid often leads to non-physical or highly inaccurate simulation results though may be solved on a very powerful solver. Hence the grid generation skills, capability and its exposure are of equal importance as much as that of the solver operations [47].

Due to the complexity of two-phase flow simulation, the numerical analysis in this investigation was implemented through the structured and unstructured grid types, in order to reach an appropriate result, compare to the experimental results, including with and without radiation effect during the combustion process.

The 3D domain of calculation in this study is shown in Fig. 4, which is the simplification of Fig. 4 designed by Ghose P. et al., for the real experiment [21; 22; 23].

Beside that the hexahedral (structured) and unstructured (tetrahedral) grids were shown in Fig. 5.

The number of nodes and elements, for hex grids are 1305600, 1287459, and the number of nodes and elements for Tet grids are 64716868, 2634984.

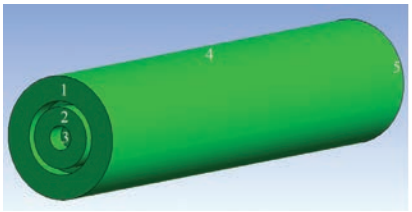

Fig. 4. 3D domain of calculation:
1 – primary air(coflow); 2 – secondary air (swirling air); 3 – the plane and centre of the injection; 4 – combustor wall; 5 – combustor outlet

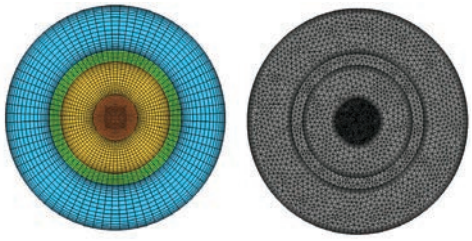

a b

Fig. 5. Grids for the numerical analysis from the air and fuel inlet section of combustor:
a – structured (hexa) grids; b – unstructured (tetra) grids

By comparison, the simulated and experimental results done by Ghose P. et al., a good agreement with the wall and the outlet temperature, were reached in this investigation which can be obtained in Fig 6. And Fig 7.

This confirms the validity of the model. However, it should be note that the obtained results on the combustor wall temperature which was implemented by P. Ghose et al., was done on a specific martial, so the wall temperature in study is the temperature inside the combustor near the inner wall, that is why the comparing results in Fig 6., show the wall temperature difference, between the real and numerical experiment. Based on the model, a mesh sensitivity analysis is constructed to investigate the flow behaviour and results during the combustion process including the radiation effects.

For further numerical study in this paper, we suggest the structured mesh with P1 radiation model, because of the good agreement with the real experiment results which was shown above in Fig 6. and Fig 7.

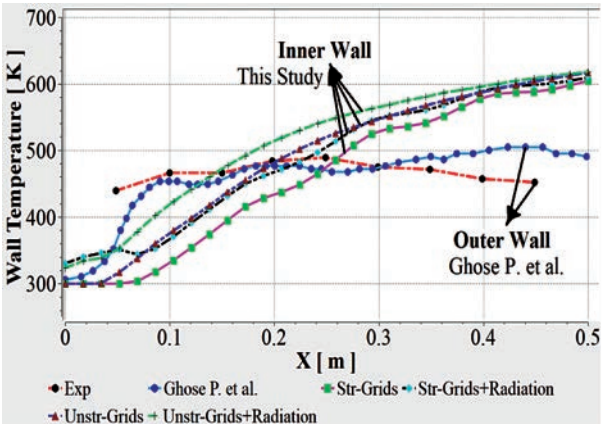

Fig. 6. Combustor wall temperature distribution obtained in real experiment done by P. Ghose et al. and numerical experiments in this study, including structed and unstructured grids, with and without radiation effect

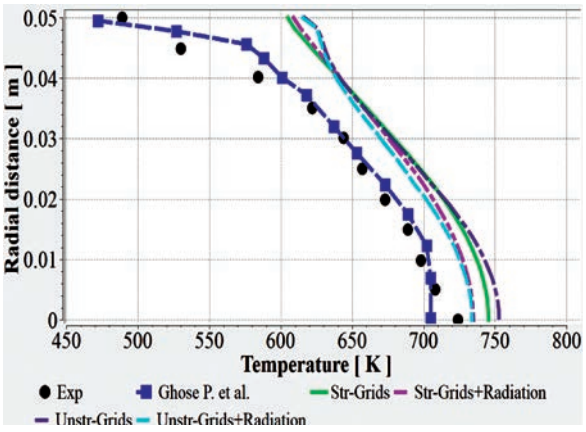

Fig. 7. Exit gas temperature distribution obtained at the outlet of combustor in real experiment done by P. Ghose et al. and numerical experiments in this study, including structed and unstructured grids, with and without radiation effect

DISCUSSION OF THE OBTAINED RESULTS
DROPLET SIZE DISTRIBUTION

The first section of this numerical analysis is the effect of the initial diameter of kerosene droplets on the temperature distribution in the combustion primary zone and at the outlet of combustor with respect to the concentration of NO and CO. The initial diameter of kerosene droplets is 18 μm, 24 μm, 40 μm, 50 μm, 57 μm and 65 μm including Rosin Rammler droplet particles size distribution with the power of 3, or distribution parameters, (q=3).

All the rest of the boundary condition are the same as boundary condition in real experiment implemented by P. Ghose et al., such as spray characteristics and primary and secondary air entering the combustor.

The general view of the fuel injection into the combustor, have shown in Fig. 8, including the areas of the investigation in the primary zone of the combustion.

All these areas of the study are started from the spray nozzle centre and show the flame characteristics such as temperature distribution and the concentration of NO and CO, in combustion primary zone. The scope of this research, is in distances of, 15 mm, 35 mm, 55 mm, 75 mm, 95 mm and 120 mm, which have the maximum of NO formation because of the maximum flame temperature.

The kerosene combustion temperature, NO and CO distributions are shown in Fig. 9, Fig. 10, and Fig 11 for the various droplet diameters in the various distance, from the centre of the injector nozzle.

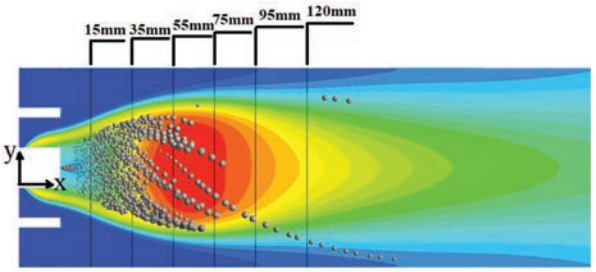

Fig. 8. The general view of fuel injection into the combustor including the specific areas of the study in combustion primary zone

Droplet sizes are, of course, of great importance in low-emissions combustion because of their strong influence on fuel evaporation rates and droplet lifetimes.

Of equal importance, however, is the symmetry of the spatial distribution of fuel within the spray. Failure to achieve a symmetrical mass flux distribution can result in local regions of mixture inhomogeneity in the combustion zone, a situation that is highly detrimental to low-emissions combustion [10].

From the obtained results in Fig. 9, Fig. 10, and Fig. 11, it is obvious that the atomization improvements and quality such as the size of the droplets, has a significant effect on many important aspects on combustion performance such as the temperature distribution, NO emission

levels and CO concentration, in the primary zone of the combustion.

Two main effects could be responsible for the observed results in Fig. 9, Fig. 10, and Fig. 11. First, an increased residence time in the post-flame gases for the finer drops relative to the larger drops could lead to increase the flame temperature, CO concentration and NO emissions. Second, the burning characteristics of the fuel

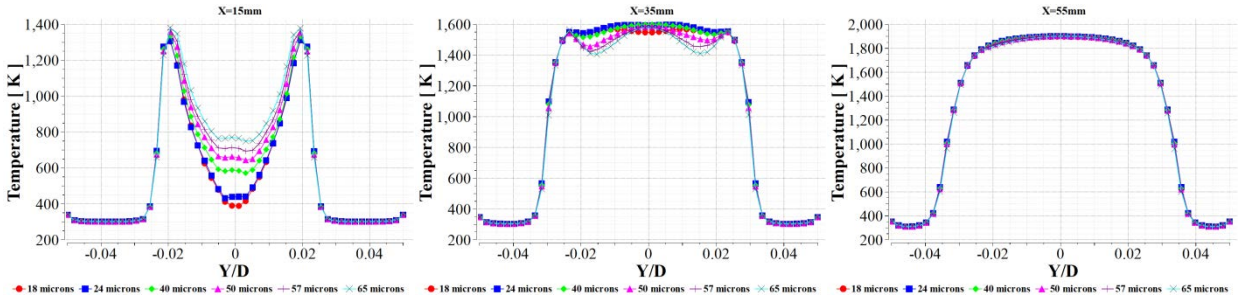

a b c

Fig. 9. Temperature distribution in the various combustion primary zone for various droplet diameters

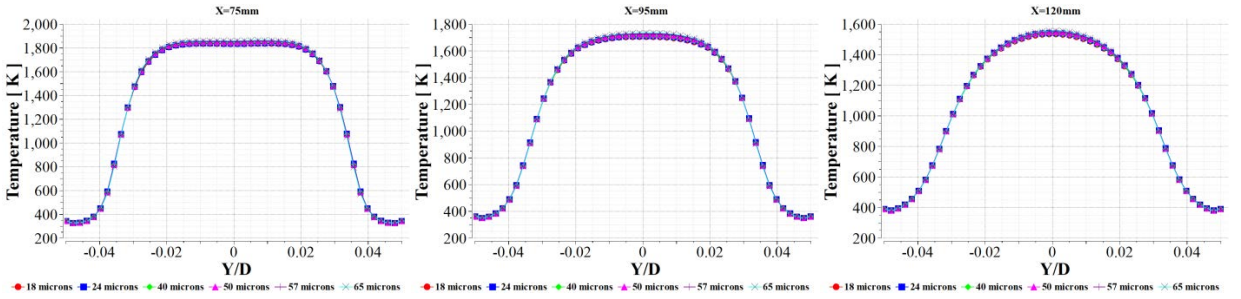

d e f

Fig. 9. Temperature distribution (continue) in the various combustion primary zone for various droplet diameters

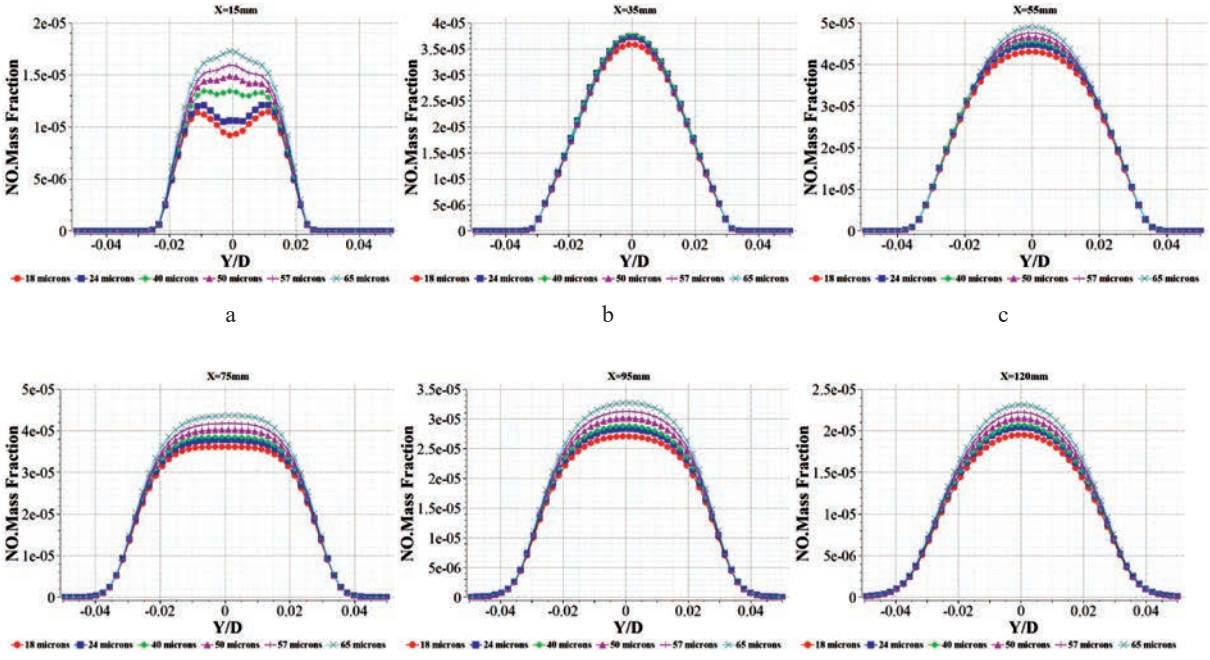

a b c

d e f

Fig. 10. NO distribution in the various combustion primary zone for various droplet diameters

droplet array may differ depending on drop size, thereby changing the flame temperature. For example, small drops may evaporate so quickly that the fuel-air mixture is almost premixed, while the mixture around larger drops is richer due to longer evaporation times.

As described above in (Fig. 9a), the minimum flame temperature in the middle of the first zone of vaporization, (15 mm) far from the centre of injector nozzle, is for the droplets with minimum diameter of 18 μm and 24 μm, which is 390K and 450K when the maximum flame

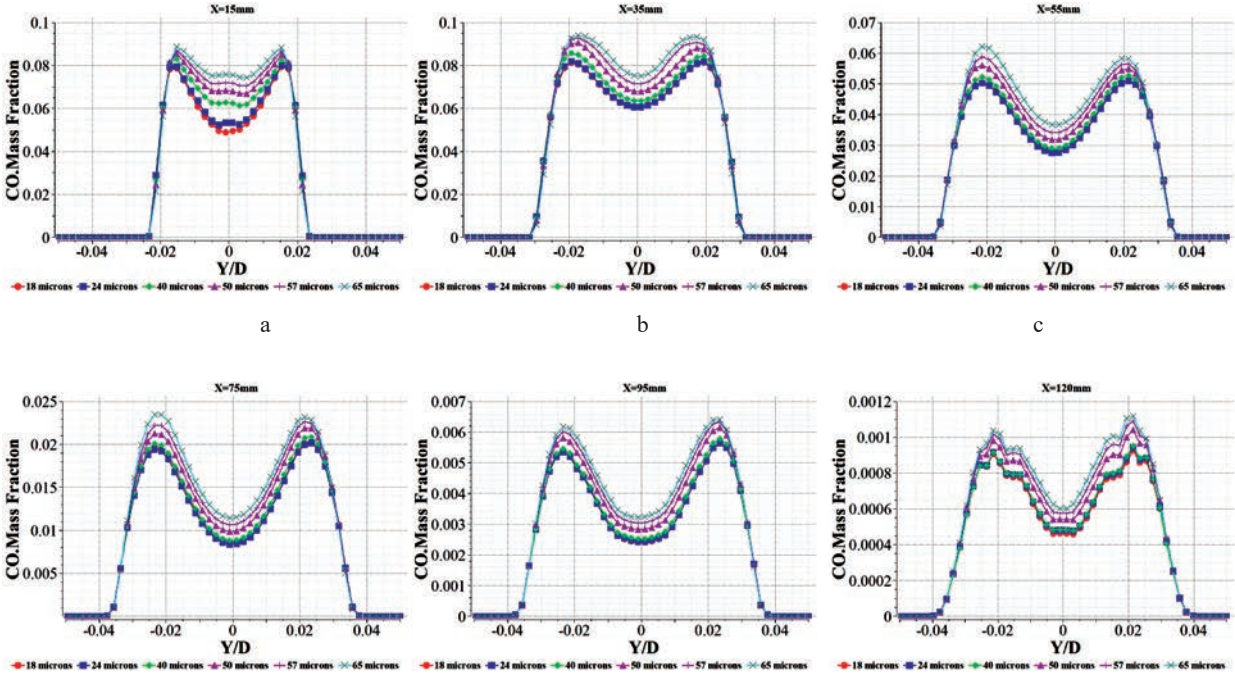

Fig. 11. CO distribution in the various combustion primary zone for various droplet diameters

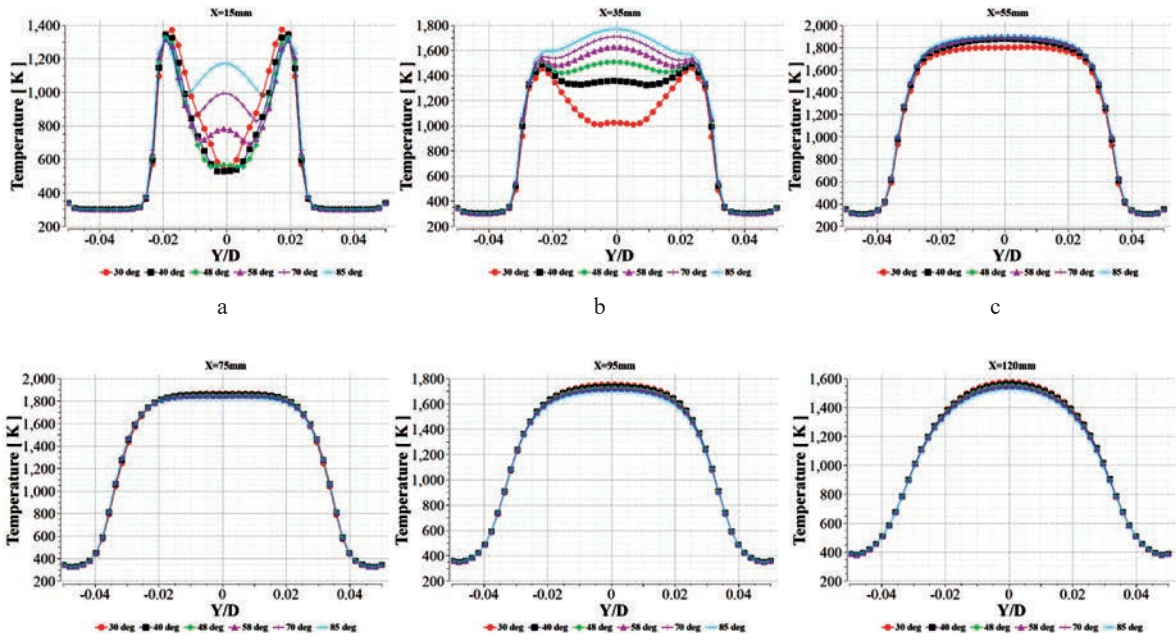

Fig. 12. Temperature distribution in the various combustion primary zone for various cone angle

temperature of 770K was obtained with the maximum droplet size of 65 μm, beside that the flame temperature with the droplets of 40 μm, 50 μm and 57 μm, have the maximum temperature, of 590K, 650K and 700K.

Numerical simulations indicate that lifetimes of 57 μm droplets are roughly several times those of 18 μm droplets. If residence time were the most important factor in determining NO formation, NO emissions should decrease with increase in droplet size, since finer fuel droplets evaporate and burn more quickly than large droplets, and thus would form more NO due to increased residence time in the hot post-flame environment.

However, when examining the Fig. 10 and Fig. 11, it is clearly evident that this is not the case. In fact, peak NO and CO levels are observed regardless of the initial drop size. This suggests that the observed increase in CO and NO emissions for large drops is due to increased local flame temperatures, not residence time.

Fig. 9b shows the post vaporized droplets in the distance of 35 mm. As it is clear that the temperature rises in this area due to a large percentage of the droplet vaporization, this causes the temperature to rise. In Fig. 9 c, d, e, f the maximum flame temperature is for the larger droplets, in mentioned areas and the finer droplets have the minimum temperature. The temperature differences in these areas are 30K between the combustion of finer and larger droplets. Considering the results obtained for the maximum temperature distribution, in mentioned areas in the combustion primary zone, it is obvious that also the maximum and the minimum formation of CO and NO, depends on the droplet sizes because the small droplets evaporate so rapidly and, due to their close spacing, mix so quickly with the surrounding air, that combustion occurs essentially as a premixed flame, which were shown in Fig. 10 and Fig. 11 (a to f). The preceding discussion suggests that improvements in atomization quality leading to reduce temperature, NO emissions and CO concentration, can be attributed to changes in flame characteristics. The exit concentration of NO and temperature at the outlet of the combustor is presented in Table 2, including the maximum temperature, time, droplet evaporation, with respect to the maximum droplet evaporation distance.

According to the Table 1 obtaining results at the outlet of the combustor can confirm the obtaining results mentioned above. Although the values of results are not significant, but the difference is felt, cause of the sensitivity of the problem.

Referring to the Table 1 because of the large diameter of the droplets in the range of 65 μm to 112 μm, the evaporation time is maximum, while the minimum is for the finer droplet range, as showed, 18 μm to 31 μm, so the droplet traveling distance and the maximum evaporation temperature for fully evaporation of droplets obey the minimum and the maximum droplet size. The average value of outlet temperature and NO distribution in Table 1 showed, that the maximum temperature of combustion products and NO concentration are for the combustion of larger kerosene droplets while the finer droplets have the minimum formation of NO because of the minimum exit flame temperature.

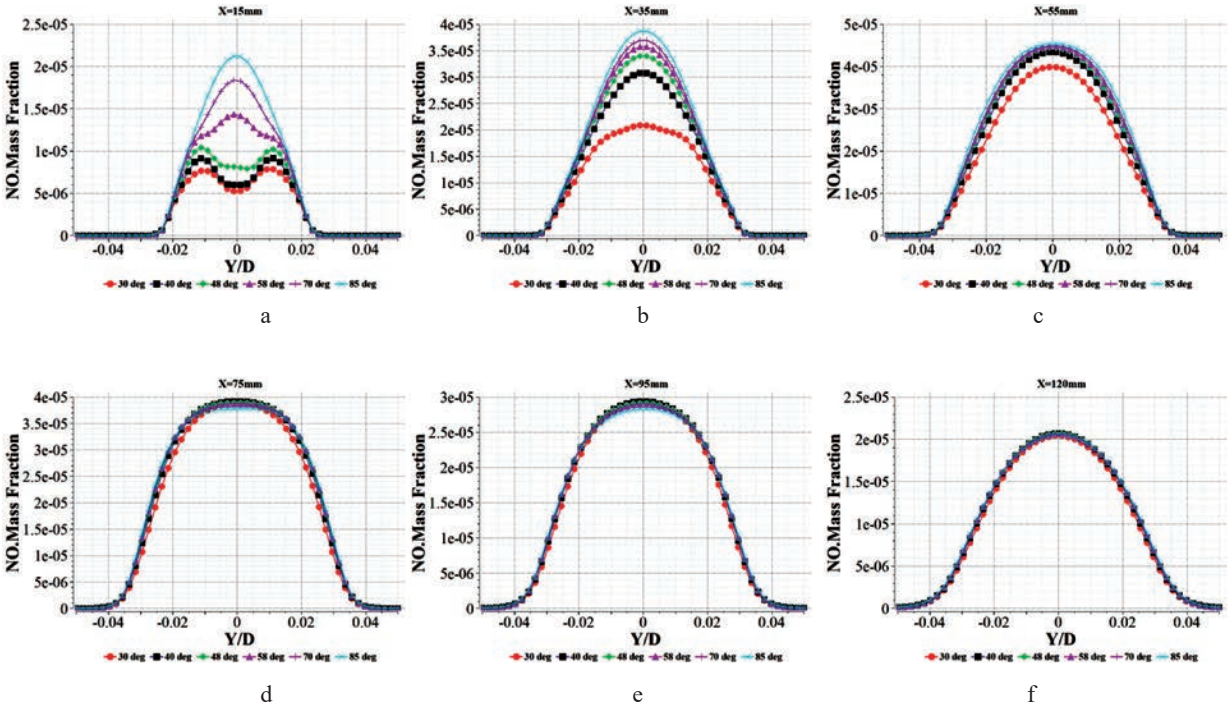

Fig. 13. NO distribution in the various combustion primary zone for various cone angle

DISCUSSION OF THE OBTAINED RESULTS
FUEL SPRAY CONE ANGLE

The droplet distribution after atomization depends on spray cone angle, hence it affects the performance of combustor [48]. The boundary conditions in this part of investigation are the same as the first part. The velocity of fuel injection is 26 m/s and the initial diameter of droplets is 24 μm. The combustion characteristic results and formation of CO and NO and temperature distribution in the combustion primary zone are presented in Fig. 12, Fig. 13 and Fig. 14 in various full cone angle of 30°, 40°, 48°, 58°, 70°, 85°.

The spray cone angle of fuel entering the combustion chamber plays an important role in overall air entrainment and the fuel-air mixing process which in turn leads to flame lift-off length and soot formation [49].

One of the important aspects of fuel spray design, in addition to achieving the desired drop-size distribution, is to ensure that the droplets formed in atomization are discharged from the nozzle in the form of a symmetrical uniform spray means, an increase in spray cone angle increases the exposure of the droplets to the surrounding air or gas, leading to improved atomization and to higher rates of heat and mass transfer [2].

Referring to the analysis of recent research and publications, it should be noted, that,Yokota and Matsuoka [50] and Hiroyasu and Arai [51] have derived correlations for their experimental data on spray angles obtained at high ambient air pressures. These and other equations for the spray cone angles of plain orifice atomizers are presented and discussed in references [52] and [51].

Ohrn et al. [53] used 40 different plain-orifice atomizers to examine the effects of nozzle geometry and flow conditions on spray cone angle. Some of their results showing the effects of nozzle pressure differential and orifice length/ diameter ratio on the cone angle for round-edged inlets. The main conclusion from their study is that the cone angle increases with injection pressure for sharp-edged and slightly radiused inlet nozzles, but

Table 1. The exit NO and temperature distribution and the characteristic of droplet evaporation

MIN and MAX droplet diameter [μm]	Average temperature @ OUTLET [K]	Average NO mass fraction @ OUTLET	MAX droplet evaporation temperature [K]	MAX droplet evaporation time [s]	MAX droplet evaporation distance [m]
18–31	658.723	2.80201e-006	398.995	0.0134682	0.0368691
24–41,5	661.001	2.90655e-006	400.882	0.0132346	0.0424017
40–69,2	658.685	2.94709e-006	406.535	0.0174998	0.0768261
50–86,5	659.096	2.9907e-006	408.107	0.0325565	0.254096
57–98,6	659.181	3.05915e-006	408.574	0.0668777	0.54225
65–112,5	659.179	3.15936e-006	409.365	0.0703071	0.568132

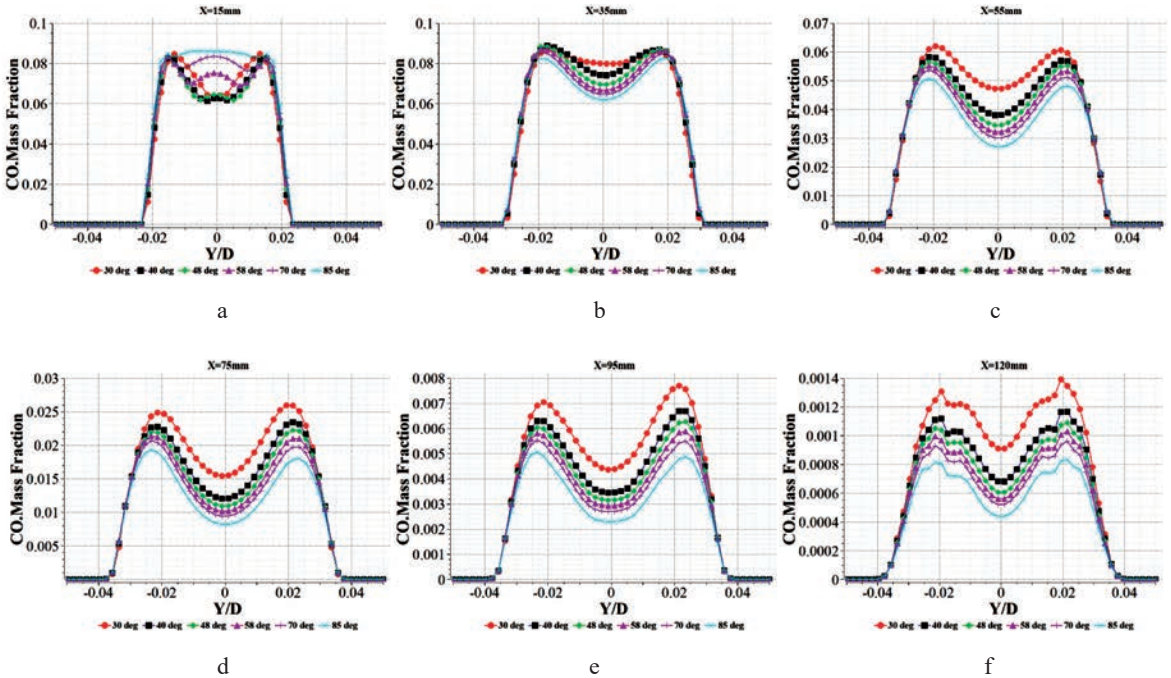

Fig. 14. CO distribution in the various combustion primary zone for various cone angle

is largely independent of injection pressure for highly radiused inlets [2].

In this part of investigation Fig. 12 a, b, c, d, e, f shows the effect of spray cone angle on the temperature distribution in the first combustion primary zone. By increasing the spray cone angles, (30°, 40°, 48°, 58°, 70°, 85°) the mixing rate between fuel droplets and oxidant increases, and this leads to an increase in temperature, but in the distances of 75 mm, 95 mm and 120 mm, not significant temperature change exists between the maximum and the minimum spray cone angle which is about 50 K, i.e., in these 3 areas, with increasing the spray cone angle, the temperature drops, due to the better mixing rate in the high temperature zone of the flame core, after almost fully vaporized droplets. This means that because of the higher spray cone angle the fuel droplets falls in the high velocity zone of gases, unlike the distances of 15 mm, 35 mm and 55 mm, which the droplets are not fully vaporize to form a complete combustion.

The maximum temperature value in Fig. 12 a, is 1175 K, for the spray cone angle of 85° while minimum value is 540 K, for the 30°, due to the reasons mentioned above, while the minimum and maximum temperature for Fig. 12 b are 1025 K and 1775 K and in Fig. 12 c are 1800 K and 1900 K respectively.

In Fig. 12 d, the temperature of 1870 K is the maximum value for the 30° spray cone angle and the minimum value of 1830 K is for the spray cone angle of 85°.

In Fig. 12 e and FIG 12 f, the temperature of 1750 K and 1580 K are the maximum values for the 30° spray cone angle and the minimum values of 1700 K and 1530 K is for the spray cone angle of 85° respectively.

As it is clear from the temperature distribution in various combustion primary zone, the NO concentrations, shown in Fig. 13 (a to f), reduce with decreasing the temperature values.

The values of NO formation in Fig. 13 (a to c) are the maximum for the spray cone angle of 85°, due to the maximum temperature and beside that the minimum is for 30° spray cone angle. The Fig. 13 (d to f) reveals that the minimum NO concentration is at 85° spray angle and 30° the maximum value. Referring to the Fig. 14 (a to f), in spite of (a), the minimum concentration of CO is for the higher spray cone angle and the maximum is for the spray cone angle with the minimum value. The CO concentrations reduce with increasing the spray

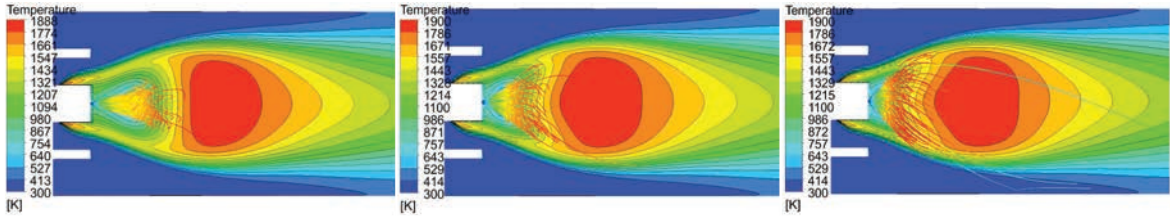

a b c

Fig. 15. Temperature distribution along the combustion primary zone including particle trajectories in various spray cone angle *a – 30°, b – 58°, c – 85°, spray cone angles*

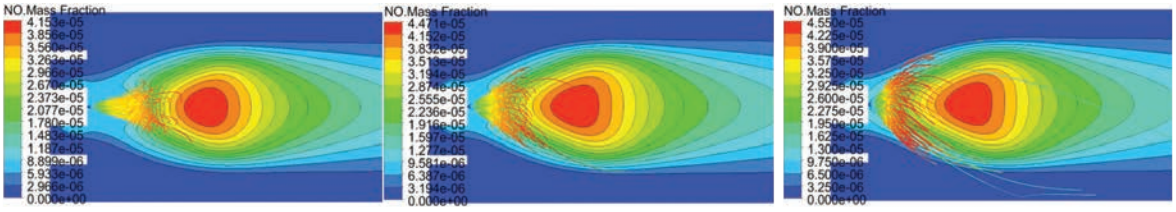

a b c

Fig. 16. NO formation distribution along the combustion primary zone including particle trajectories in various spray cone angle

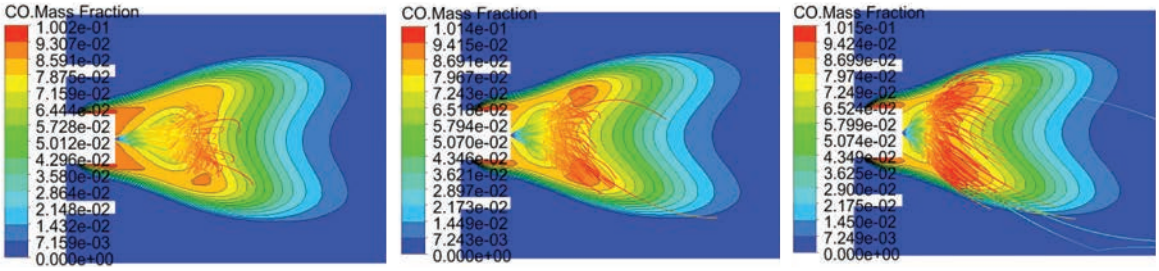

a b c

Fig. 17. CO formation distribution along the combustion primary zone including particle trajectories in various spray cone angle *a – 30°, b – 58°, c – 85°, spray cone angles*

Table 2. The exit NO and temperature distribution and the characteristic of droplet evaporation

Injection angle [deg]	Average temperature @ OUTLET [K]	Average NO mass fraction @ OUTLET	MAX droplet evaporation temperature [K]	MAX droplet evaporation time [s]	MAX droplet evaporation distance [m]
30	658.946	2.6108e-006	406.978	0.00569393	0.0563126
40	658.904	2.76713e-006	406.947	0.00509002	0.0531599
48	659.019	2.82902e-006	407.092	0.0050277	0.0531484
58	658.998	2.87104e-006	407.322	0.00498542	0.0568473
70	659.043	2.91454e-006	405.386	0.00505006	0.0682121
85	659.027	2.99638e-006	403.551	0.0143817	0.197561

cone angles. The Fig. 14 reveals that the minimum CO concentration is at 85° spray cone angle because increasing the spray angle produces lower fuel droplet diameter. Increasing the mixing rates between fuel and air drops resulted in a homogenous mixture which increased flame temperature. The Fig. 14 a show that in the first zone of droplet evaporation, not complete mixing rate and combustion occur, and du to this reason the concentration of CO is maximum for the maximum spray cone angle of 85°.The flame characteristics including the droplet trajectories, temperature distribution, formation of NO and CO, are presented in Fig. 15 to Fig. 16, along the combustion primary zone for 30°, 58°, 85° cone angles.

In this CFD numerical analysis, the results in Fig.15 to Fig. 17 show the temperature distribution in the middle plane of combustor and the droplet traveling way in the combustion primary zone for the 3 various spray cone angles.

The main purpose of Fig.15 to Fig. 17 is to show the behaviour of CO, NO and temperature in the main zone of the flame core, which are formed as clear.

According to the Table 2 obtaining results at the outlet of the combustor are presented.

Referring to the Table 2 because of the large spray cone angle in the range 30° to 85°, the maximum evaporation time and evaporation distance is for the spray cone angle of 85°, while the minimum is for the angles 30°, 40°, 48°, 58°, 70°.

Besides that, the minimum droplet evaporation temperature is for the cone angle of 85° which is 403.5 while for the 30°, 40°, 48°, 58°, 70°, is maximum.

The average value of outlet temperature and NO distribution showed, that the maximum temperature of combustion products and NO concentration are for the combustion of kerosene with the large spray cone angles.

CONCLUSIONS

Fuel injection preparation is of vital importance in the attainment of low pollutant emissions. Future advances in low-emissions combustion technology will demand a detailed knowledge of the properties and structure of the sprays.

The properties of prime interest include drop size distributions, the spray cone and droplet trajectories.

Such detailed information is essential for the successful modelling of fuel sprays, but the extent to which predictions based on spray models can be utilized in combustor design depends largely upon the degree to which they can be validated or refuted by accurate experimental data. This situation calls for more collaborative efforts between the simulation and experimentation communities.

Current CFD numerical simulation investigated the effect of initial kerosene droplet diameters, (18 μm to 65 μm) and spray cone angles (30° to 85°) on the characteristics of the flame in the combustion primary zone, such as formation of NO emissions, concentration of CO and temperature distribution. Also, the behaviour of these characteristics was shown at the outlet of the combustor.

The method of Eulerian-Lagrangian approach was used to investigate the dispersion and the evaporation of kerosene droplets by means of flamelet model of combustion, including the simulation of thermal and prompt formation of NO. For validation of using combustion model, comparison of computational results with experimental results shows good agreement. The results show that, by increasing the droplet sizes, temperature, NO emission levels and CO concentration rise, in combustion primary zone and at the outlet of combustor, due to the quality of mixing rate. On the other hand, as the results show, the emissions are influenced of spray cone angle. Increasing the fuel spray cone angle causes to increase the temperature and NO concentration in combustor output. It should be noted that in the combustion primary zone, by increasing the spray cone angle the CO concentration gives the lower value, except in the distance of 15 mm, due to the not fully vaporized droplets, so this leads to a weak mixing rate. So, by increasing the spray cone angle the NO concentration and temperature value rise in the distances (15 mm, 35 mm and 55 mm), while these values are lower in the distances (75 mm, 95 mm and 120 mm), due to the mixing quality and not fully droplet vaporization in the first 3 areas of combustion primary zone, which mentioned above.

Atomization quality, such as the initial diameter of droplets and spray cone angle, affects emission levels

through the evaporation and mixing characteristics of the spray, as investigated in this study. Generally, the influence of atomization quality is most definite at slightly fuel-lean conditions, with reduced initial drop sizes and cone angle of spray leading to decreased emissions. This reduction in emissions is attributed to the more uniform fuel dispersion and higher evaporation rates that are characteristic of small drops, and which cause a larger proportion of the total burning process to occur in a premixed, rather than a diffusion, mode.

REFERENCES

[1] Eckert, P., & Rakowski, S. (2012). Pollutant Formation. In G.P. Merker, C. Schwarz, & R. Teichmann (Eds.), *Combustion Engines Development: Mixture Formation, Combustion, Emissions and Simulation* (pp. 193–223). Springer Berlin Heidelberg. Retrieved from: https://doi.org/10.1007/978-3-642-14094-5_6.

[2] Lefebvre, A. H., & Ballal, D. R. (2010). Gas Turbine Combustion: Alternative Fuels and Emissions, Third Edition (3rd ed.). CRC Press. Retrieved from: https://doi.org/10.1201/9781420086058.

[3] Albin T., da Franca A. A., Varea E., Kruse S., Pitsch H., Abel D. (2015). Potential and Challenges of MILD Combustion Control for Gas Turbine Applications. In: King R. (eds) *Active Flow and Combustion Control 2014*. Notes on Numerical Fluid Mechanics and Multidisciplinary Design, Vol. 127. Springer, Cham. Retrieved from: https://doi.org/10.1007/978-3-319-11967-0_12.

[4] Correa, S. M. (1993). A Review of NOx Formation Under Gas-Turbine Combustion Conditions. *Combustion Science and Technology*, *87*(1–6), 329–362. Retrieved from: https://doi.org/10.1080/00102209208947221.

[5] Correa, S. M., Sanjay, M. (1991). "Lean Premixed Combustion for Gas-Turbines: Review and Required Research", *Proceedings of the 14th Annual Energy-Sources Technology Conference and Exhibition*, Anonymous Publ by ASME, New York, NY, USA, Houston, TX, USA, 33, pp. 1–9.

[6] Brewster, B. S., Cannon, S. M., Farmer, J. R., & Meng, F. (1999). Modelling of lean premixed combustion in stationary gas turbines. *Progress in Energy and Combustion Science*, *25*(4), 353–385. Retrieved from: https://doi.org/10.1016/S0360-1285(98)00014-8.

[7] Angello, L, & Lowe, P. "Dry Low NOx Combustion Development for Electric Utility Gas Turbine Applications: A Status Report". Proceedings of the ASME 1989 International Gas Turbine and Aeroengine Congress and Exposition. Volume 3: Coal, Biomass and Alternative Fuels; Combustion and Fuels; Oil and Gas Applications. Toronto, Ontario, Canada. June 4–8, 1989. V003T06A008. ASME. Retrieved from: https://doi.org/10.1115/89-GT-254

[8] Bowman, C. T. (1992). Control of combustion-generated nitrogen oxide emissions: Technology driven by regulation. *Symposium (International) on Combustion*, *24*(1), 859–878. Retrieved from: https://doi.org/10.1016/S0082-0784(06)80104-9.

[9] Kelkar, A., Ramakrishna, C., Sivathanu, Y., & Gore, J. (n.d.). Temperature and velocity statistics of lean premixed jet flames for NO(x) calculations. In *34th Aerospace Sciences Meeting and Exhibit*. Retrieved from: https://doi.org/10.2514/6.1996-818.

[10] Lefebvre, A. H. (1995). The Role of Fuel Preparation in Low-Emission Combustion. *Journal of Engineering for Gas Turbines and Power*, *117*(4), 617–654. Retrieved from: https://doi.org/10.1115/1.2815449.

[11] Lefebvre, A., & Mcdonell, V. (2017). Atomization and Sprays. In *Atomization and Sprays*. Retrieved from: https://doi.org/10.1201/9781315120911.

[12] Rink, K. K., & Lefebvre, A. H. (1989). The Influences of Fuel Composition and Spray Characteristics on Nitric Oxide Formation. *Combustion Science and Technology*, *68*(1–3), 1–14. Retrieved from: https://doi.org/10.1080/00102208908924066.

[13] Nizami, A. A., & Cernansky, N. P. (1979). NOx formation in monodisperse fuel spray combustion. *Symposium (International) on Combustion*, *17*(1), 475–483. Retrieved from: https://doi.org/10.1016/S0082-0784(79)80048X.

[14] Nizami, A. A., Singh, S., & Cernansky, N. P. (1982). Formation of Oxides of Nitrogen in Monodisperse Spray Combustion of Hydrocarbon Fuels. *Combustion Science and Technology*, *28*(3–4), 97–106. Retrieved from: https://doi.org/10.1080/00102208208952546.

[15] Moesl, K. (2012). *On the Formation of Nitrogen Oxides During the Combustion of Partially Pre-Vaporized Droplets*. PhD Thesis.

[16] Fossi, A. A. (2017). *Numerical simulation of stationary and transient spray combustion for aircraft gas turbine applications*. PhD Thesis. Retrieved from: http://hdl.handle.net/20.500.11794/27597.

[17] Abrishamchi, I. and Khazraii, Y., Bashirnezhad, K. (2014). "Effect of fuel spray angle on pollutants emission in turbulent spray flames", M.Sc. Thesis, Department of Mechanical Engineering, Mashhad Azad University, Mashhad, I.R. Iran.

[18] Yasamin Khazraii, Keyvan Daneshvar, and Hossein PoorkhademNamin (2011). "Numerical Simulation on NO_x Emission in Liquid Fuel Spray Flames". *International Journal of Modelling and Optimization.* Vol. 1, No. 4, pp. 334–339. Retrieved from: https://doi.org/10.7763/IJMO.2011.V1.57.

[19] Mishra, R. K., Kumar, S. Kishore and Chandel, Sunil. (2016). "Effect of Spray Cone Angle on Flame Stability in an Annular Gas Turbine Combustor". *International Journal of Turbo & Jet-Engines*, Vol. 33, No. 1, pp. 35–44. Retrieved from: https://doi.org/10.1515/tjj-2015-0006.

[20] Hajivand, M. (2015). CFD modelling of kerosene combustion with various initial conditions and fuel droplet diameters. *Energy and heat engineering processes and equipment*. Kharkov, NTU, KhPI. № 16 (1125). Pp. 54–66. Retrieved from: http://repository.kpi.kharkov.ua/handle/KhPI-Press/17609.

[21] Ghose, P., Patra, J., Datta, A., & Mukhopadhyay, A. (2016). Prediction of soot and thermal radiation in a model gas turbine combustor burning kerosene fuel spray at different swirl levels. *Combustion Theory and Modelling*, 1–29. Retrieved from: https://doi.org/10.1080/13647830.2016.1147607.

[22] Ghose, P., Patra, J., Datta, A., & Mukhopadhyay, A. (2014). Effect of air flow distribution on soot formation and radiative heat transfer in a model liquid fuel spray combustor firing kerosene. *International Journal of Heat and Mass Transfer*, *74*, 143–155. Retrieved from: https://doi.org/Retrieved from: https://doi.org/10.1016/j.ijheatmasstransfer.2014.03.001.

[23] Ghose, P., Datta, A., Ganguly, R., Mukhopadhyay, A., & Sen, S. (2018). Modelling of Soot Formation in a Kerosene Spray Flame BT – *Modelling and Simulation of Turbulent Combustion* (S. De, A.K. Agarwal, S. Chaudhuri, & S. Sen (eds.); pp. 363–394). Springer Singapore. Retrieved from: https://doi.org/10.1007/978-981-10-7410-3_12.

[24] CFX. *ANSYS CFX-Solver Modelling Guide*, ANSYS, Inc., Canonsburg, PA, USA, Release 18.2.

[25] CFX. *ANSYS CFX-Solver Theory Guide*, ANSYS, Inc., Canonsburg, PA, USA, Release 18.2.

[26] Jones, W. P. & Launder, Brian. (1973). The Prediction of Laminarization with a Two-Equation Model of Turbulence. Intj. Heat Mass Transfer. 5. 301 314.

[27] Zimmermann, I. (2009). *Modelling and Numerical Simulation of Partially Premixed Flames* [Universität der Bundeswehr München, Fakultät für Luft- und Raumfahrttechnik]. Retrieved from: .

[28] Acharya, R. (2016). *Investigation of Differences in Ansys Solvers CFX and Fluent* (Dissertation). Retrieved from: http://urn.kb.se/resolve?urn=urn:nbn:se:kth:diva-203937.

[29] Khayamyan, S. (2010). *Flow field in a gas turbine burner* (Dissertation). Retrieved from: http://urn.kb.se/resolve?urn=urn:nbn:se:ltu:diva-44609.

[30] Muela Castro, J. (2018). *Modelling and numerical simulation of combustion and multi-phase flows using finite volume methods on unstructured meshes*. Tesi doctoral, UPC, Departament de Màquines i Motors Tèrmics, 2018. Retrieved from: http://hdl.handle.net/2117/117638.

[31] Arima, T. (2006). Numerical Methods for Chemically Reacting Fluid Flow Computation under Low-Mach Number Approximation. *Tokyo Journal of Mathematics*, *29*(1), 167–198. Retrieved from: https://doi.org/10.3836/tjm/1166661873.

[32] Hamedi, N. (2012). *Numerical Study of NOx and Flame Shape of a DLE Burner* (Dissertation). Retrieved from: http://urn.kb.se/resolve?urn=urn:nbn:se:liu:diva-86412.

[33] Pohl, S., Jarczyk, M., Pfitzner, M., & Rogg, B. (2013). Real gas CFD simulations of hydrogen/oxygen supercritical combustion. *EUCASS Proceedings Series*, *4*, 583–614. Retrieved from: https://doi.org/10.1051/eucass/201304583.

[34] Peters, N. (2000). *Turbulent Combustion*. Cambridge University Press. Retrieved from: https://doi.org/10.1017/CBO9780511612701.

[35] Golder, Santu & Doom, Jeffrey. (2017). *Simulation of an ethylene flame with turbulence, soot and radiation modeling*. Retrieved from: https://doi.org/10.2514/6.2017-0540.

[36] Modest, M. F. (2013). *Radiative Heat Transfer.* Elsevier Science. Retrieved from: https://books.google.com.ua/books?id=J2KZq0e4lCIC.

[37] Storakach, E. A., Borovik, I. N., Bazarov, V. G., & Haidn, O. J. (2020). Numerical study of operational processes in a GOx-kerosene rocket engine with liquid film cooling. *Propulsion and Power Research*, *9*(2), 132–141. Retrieved from: https://doi.org/10.1016/j.jppr.2020.04.004.

[38] Höglauer, C., Kniesner, B., Knab, O. et al. (2015). Modelling and simulation of a GOX/kerosene subscale rocket combustion chamber with film cooling. *CEAS Space J* 7, 419–432 Retrieved from: https://doi.org/10.1007/s12567-015-0096-y.

[39] Reid, R. C., Prausnitz, J. M., & Poling, B. E. The properties of gases and liquids. United States. Retrieved from: https://www.osti.gov/biblio/6504847.

[40] Ghose, P., Datta, A., and Mukhopadhyay, A. (November 11, 2015). "Effect of Prediffuser Angle on the Static Pressure Recovery in Flow Through Casing-Liner Annulus of a Gas Turbine Combustor at Various Swirl Levels". ASME. *J. Thermal Sci. Eng. Appl*. March 2016; 8(1): 011017. Retrieved from: https://doi.org/10.1115/1.4030734.

[41] Morsi, S., & Alexander, A. (1972). An investigation of particle trajectories in two-phase flow systems. *Journal of Fluid Mechanics, 55*(2), 193–208. Retrieved from: https://doi.org/10.1017/S0022112072001806.

[42] Ranz, W.E., Marshall, W.R (1952). Evaporation from drops: Part II. Chemical Engineering Progress, 48, pp. 173–180.

[43] Zhukov, V. P. (2012). Verification, Validation, and Testing of Kinetic Mechanisms of Hydrogen Combustion in Fluid-Dynamic Computations. *ISRN Mechanical Engineering,* 475607. Retrieved from: https://doi.org/10.5402/2012/475607.

[44] Warnatz, J., Maas, U., & Dibble, R. (2006). *Combustion: Physical and Chemical Fundamentals, Modeling and Simulation, Experiments, Pollutant Formation*. Retrieved from: https://doi.org/10.1007/978-3-540-45363-5.

[45] Ravikanti, M., Hossain, M., & Malalasekera, W. (2009). Laminar flamelet model prediction of NOx formation in a turbulent bluff-body combustor. *Proceedings of the Institution of Mechanical Engineers, Part A: Journal of Power and Energy*, *223*(1), 41–54. Retrieved from: https://doi.org/10.1243/09576509JPE569.

[46] Jiang, B., Liang, H., Huang, G., & LI, X. (2006). *Study on NOx Formation in CH4/Air Jet Combustion. Chinese Journal of chemical engineering,* 14(6), 723–728. Retrieved from: https://doi.org/10.1016/S1004-9541(07)60002-0.

[47] Basics of grid generation for the CFD analysis. Retrieved from: https://www.learncax.com/knowledge-base/blog/by-category/cfd/basics-of-grid-generation-for-cfd analysis#:~:text=Grid%20generation%20or%20meshing%20is,of%20results%20of%20the%20study.

[48] Kulshreshta, D., & Channiwala, S.A. (2018). Factors Affecting Spray Cone Angle of Pressure Swirl Atomizer for Gas Turbine Combustion Chamber: Theoretical and Experimental Analysis. *Indian Journal of Science and Technology*, *11*, 1–4. Retrieved from: https://doi.org/10.17485/ijst/2018/v11i8/118123.

[49] Tang, M. (2018). *Spray and Combustion Studies of High Reactivity Gasoline in Comparison to Diesel under Advanced Compression Ignition Engine Conditions*. Open Access Dissertation, Michigan Technological University. Retrieved from: https://doi.org/10.37099/mtu.dc.etdr/686.

[50] Yokota, K., & Matsuoka, S. (1977). An Experimental Study of Fuel Spray in a Diesel Engine. *Transactions of the Japan Society of Mechanical Engineers*, *43*(373), 3455–3464. Retrieved from: https://doi.org/10.1299/kikai1938.43.3455.

[51] Hiroyasu, H., & Arai, M. (1990). Structures of Fuel Sprays in Diesel Engines. *SAE Transactions, 99*, 1050–1061. Retrieved April 3, 2021, from http://www.jstor.org/stable/44548562.

[52] Lefebvre, A. H., & McDonell, V. G. (2017). *Atomization and sprays* (2nd ed.). CRC Press. Retrieved from: https://doi.org/10.1201/9781315120911.

[53] Ohrn, T. R., Senser, D. W., & Lefebvre, A. H. (1991). Geometrical effects on discharge coefficients for plain-orifice atomizers. *Atomization and Sprays*, *1*(2). Retrieved from: https://doi.org/10.1615/AtomizSpr.v1.i2.10.

Дата надходження статті до редакції: 11.03.2021
Дата затвердження статті до друку: 25.03.2021